DANGER OF ZOOPLANKTON FEEDING: THE FLUID SIGNAL GENERATED BY AMBUSH FEEDING COPEPODS

Thomas Kiørboe

National Institute of Aquatic Resources, Technical University of Denmark, Kavalergården 6, DK-2920 Charlottenlund, Denmark. Email: tk@aqua.dtu.dk

Houshuo Jiang

Department of Applied Ocean Physics and Engineering, Woods Hole Oceanographic Institution, Woods Hole, MA 02543, USA

Sean P. Colin

Environmental Sciences and Marine Biology, Roger Williams University, Bristol, RI 02809, USA

Abstract. Zooplankton feed in either of three ways: they generate a feeding current, cruise through the water, or they are ambush feeders. Each mode generates different hydrodynamic disturbances and hence exposes the grazers differently to mechanosensory predators. Ambush feeders sink slowly and therefore perform occasional upward repositioning jumps. We quantified the fluid disturbance generated by repositioning jumps in a mm-sized copepod (Re ~ 40). The kick of the swimming legs generates a viscous vortex ring in the wake; another ring of similar intensity but opposite rotation is formed around the decelerating copepod. A simple analytical model, that of an impulsive point force, properly describes the observed flow field as a function of the momentum of the copepod, including the translation of the vortex and its spatial extension and temporal decay. We show that the time-averaged fluid signal and the consequent predation risk is much less for an ambush feeding than a cruising or hovering copepod for small individuals, while the reverse is true for individuals larger than about 1 mm. This makes inefficient ambush feeding feasible in small copepods and is consistent with the observation that ambush feeding copepods in the ocean are all small, while larger species invariably use hovering or cruising feeding strategies.

Key words: viscous vortex ring, copepod jump, *Acartia tonsa*, optimal foraging

INTRODUCTION

Zooplankton feed in one of three different principal modes: they can cruise through the water while searching for prey, they may generate a feeding current and capture prey arriving in this current, or they may be ambush feeders sitting motionless in the water while waiting for prey to pass through their dining sphere, only occasionally performing upwards jumps to compensate for their slow sinking (Kiørboe 2010). Each of these feeding modes produce different hydrodynamical disturbances in the ambient water and thus cause different exposures to predators because many zooplankton predators perceive their prey by the hydrodynamical disturbance that the prey produces (Feigenbaum & Reeve 1977, Jakobsen et al. 2006, Jiang & Paffenhöfer 2008). Hence, the advantages that a zooplankter achieves from a particular feeding behavior should be traded off against the costs, including the predation risk that it entails.

The continuous fluid signals produced by cruising and feeding current foragers are rather well understood in both unicellular (Langlois et al. 2009, Leptos et al. 2009) and larger metazoan zooplankters (Catton et al. 2007; Malkiel et al. 2003, Jiang et al. 2002, Visser 2001) whereas the short-lasting instantaneous fluid signals produced by jumps have not been well studied. Jumps are a common component of the motility repertoire of many plankters (Jakobsen et al. 2006, Fenchel & Hansen 2006). Planktonic copepods, the dominating group of mesozooplankton in the ocean, jump to escape predators (Fields & Yen 1996), to attack prey (Jiang & Paffenhöfer 2008; Kiørboe et al. 2009) or to reposition in the water column (Svensen & Kiørboe 2000). While the latter jumps are obviously less powerful than the former (Buskey et al. 2002), they may be much more frequent. Thus, ambush feeders typically reposition by jumping upwards every 1-10 seconds (Tiselius & Jonsson 1990; Titelman & Kiørboe 2003). As a result, the frequent weak repositioning jumps may create a hydrodynamic signal that may expose ambush feeders to a significant predation risk (Tiselius et al. 1997).

With the aim of evaluating the predation risk associated with the 3 principal feeding modes, we examined the fluid disturbances generated by repositioning jumps of the copepod *Acartia tonsa*. Ambush feeding is common among smaller pelagic copepods, mainly within the genus *Oithona* (e.g. Paffenhöfer 1993), while feeding-current feeding and cruising dominate among larger species.

It is well established that copepods performing strong escape jumps at Reynolds numbers (Re) > 100 generate toroidal vortices in their wake (Yen & Strickler 1996, Duren & Videler 2003). Vortex formation is indeed an inescapable consequence of any unsteady motion in water occurring at high Reynolds numbers (Dickinson 1996) and has consequently been much studied in the context of animal propulsion in fluid media at Re > 100 and by applying inviscid theory (Dabiri 2009). We show here that even weak repositioning jumps (Re 20-100) generate two viscous vortex rings, one vortex in the wake of the copepod and one vortex around the decelerating body. These viscous vortex rings are formed due to the application of short-lasting localized momentum sources (e.g. Afanasyev (2004)), which is a different mechanism from flow separation such as the formation of a Kármán vortex street. We quantify the intensity of the fluid signal using Particle Image Velocimetry (PIV) and use a simple analytical viscous vortex ring model and scaling arguments to demonstrate that ambush feeding reposition jumps expose small copepods to a much lower predation risk than other feeding modes, whereas the reverse is true for copepods larger than about 1 mm.

MATERIAL AND METHODS

Copepods, *Acartia tonsa* (prosome length 0.7 – 1.1 mm), were collected in November and December in Woods Hole, MA, USA at sea temperatures of 6-10 ºC and allowed to acclimate to room temperature overnight (20 ºC). Observations for flow visualization (PIV) were made in small aquaria (~100 ml) with about 20 copepods and sufficient 5-µm tracer particles to make the water slightly cloudy. A vertical laser sheet was oriented through the aquarium. We used either a 1-W red

continuous laser (200 μs shutter time) or a 45-W pulsed green laser with a 150-ns pulse duration (Photonics Industries DM30-527). High-speed, high resolution (1024 X 1024 pixels) video recordings (1000 Hz) were made through a horizontally oriented dissecting microscope fitted with a Photron Fastcam 1024 PCI camera. The field of view was ca. 1 x 1 cm^2.

Of the many jumps observed we selected 16 jumps that occurred in the plane of the laser sheet and perpendicular to the view direction and with the copepod oriented with its side towards the camera; no jumps were perfect in this respect. In some cases (4), the copepod jumped out of the field of view allowing us to analyze only the jump wake. The jumps analysed were only the relatively weak reposition jumps described by Kiørboe et al (2010). Unavoidable advection in the aquarium rarely allowed us to analyze induced flow velocities < 1 mm s^{-1}. Copepod prosome lengths were measured on the video, and copepod masses were estimated from their volumes assuming the shape of a prolate spheroid with an aspect ratio 0.38. We assumed the mass density of the copepod and the water both to be 1 mg mm^{-3}. We estimated the maximum linear momentum of the copepod, *M*, as the product of its peak velocity and its mass and its (maximum) Reynolds number from its peak velocity and its body width.

Video sequences were analyzed using standard PIV software (LaVision, DaVis 7) to get instantaneous velocity and vorticity fields, as well as movies hereof. Time-integrated velocity and vorticity fields were computed in MatLab. Jump kinematics were analysed using ImageJ that was also used to compute the circulation of vortex rings. The circulation of a vortex ring is equal to the vorticity integrated in a meridional plane over the extension of the ring

$$\Gamma(t) = \int \omega(x, y, t) dx dy \qquad (1)$$

where $\omega(x,y,t)$ is the vorticity at position x,y at time t. In ImageJ the selected ring was cropped and the picture thresholded at various vorticities, 1, 3, 5, 10, 15,…. 50 s^{-1} and the extension areas

($A_{\omega(I,t)}$) within each threshold vorticity estimated. The circulation at each time step was then estimated as

$$\Gamma(t) = \sum_{\omega(i,t)} \omega(i,t)(A_{\omega(i,t)} - A_{\omega(i+1,t)}) \quad (2)$$

Areas with flow velocity magnitude exceeding U^* threshold velocities were estimated in a similar manner after subtraction of background flow magnitudes. Finally, we quantified the temporal change in the position of the maximum vorticity as the centre of mass of the 5 s^{-1} contour line (identified automatically by ImageJ).

THEORY

The jumping copepod leaves a vortex in its wake, generated by the backward power stroke of the swimming legs. In order to analyze this vortex and allow us to extrapolate our observations to copepods of other sizes and jumps of other intensities, we apply a simple analytical model of a viscous vortex ring generated by an impulsive point force, an idealized description of the near instantaneous power kick of the swimming legs. Here we provide enough detail for the reader to follow the arguments, but refer the main derivations to Electronic Appendix A1.

The point force acts impulsively and imparts locally a finite momentum ρI to the fluid, where ρ is the mass density of the fluid and I the hydrodynamic impulse (L^4T^{-1}). The resulting backward jet forms a vortex ring, and the circulation of this ring subsequent to a virtual time origin t_0 decays as (Eq. A5 in Appendix A)

$$\Gamma(t) = \frac{I}{4\pi\nu(t-t_0)} \quad (3)$$

where υ is the kinematic viscosity of the fluid.

Rheotactic predators perceive prey from the fluid velocity that the prey generates and respond to velocities that exceed a critical magnitude, U^* (Kiørboe & Visser 1999). We are thus interested in quantifying the extension of the region within which the induced flow velocity magnitude exceeds this critical value (U^*). Right after the jump is initiated it follows from (A11, A12) that the maximum area of the vortex in the meridional plane with velocity magnitudes exceeding U^* scales as

$$Area(U^*) \propto R_x^* \cdot R_r^* \propto (I/U^*)^{2/3}, \tag{4}$$

and from (A13) that the time t^* after which the whole flow field is below the threshold velocity is

$$t^* = \frac{1}{4\nu\pi}\left(\frac{2}{3}\frac{I}{U^*}\right)^{2/3}. \tag{5}$$

The vortex ring will expand radially due to diffusion and translate downstream due to advection and the combined drift (A17, $\Delta x(t)$) and diffusion (A14, $r_\omega(t)$) of the vorticity maximum leads to a total time- dependent distance of the vorticity maximum to the point of origin subsequent to a virtual time origin t_0

$$L(t) = a_0 + (r_\omega(t)^2 + \Delta x(t)^2)^{0.5} = a_0 + \left(2\nu(t-t_0) + \left(\frac{2I}{\pi}\right)^{1/2}(t-t_0)^{1/2}\right)^{1/2}, \tag{6}$$

where a_0 is the distance travelled from t_0 till the vortex ring can be identified in the flow field.

RESULTS

Jump kinematics, flow- and vorticity fields

A repositioning jump is initiated by the copepod sequentially striking backwards each of the 4 pairs of swimming legs while accelerating the body forward to a peak velocity of 100-200 mm s^{-1}, reached after 10-25 ms at the end of the power stroke (Fig. 1A). During the subsequent leg-recovery, the copepod coasts at a decelerating velocity and comes to an almost complete stop after another 10-25 ms. In some jumps, this beat cycle may be repeated several times (applies mainly to escape jumps). All jumps follow this scheme, although the detailed characteristics of the individual jumps with respect to duration of the power stroke and peak velocity vary (Table 1). The Reynolds numbers of the examined repositioning jumps varied between 20 and 100 and the momentum of the copepod at its peak velocity ranged from 5 to 30 mg mm s^{-1} (Table 1).

The power stroke of the swimming legs sends a jet of water backwards, which forms a vortex ring, evident in the 2D plane as two counter-rotating eddies (Fig. 2; Appendix movie 1). Another counter-rotating ring forms around the body of the decelerating copepod.

The wake vortex: Formation, extent, translation, decay

During and subsequent to the jump, the vortex in the wake of the copepod forms and grows (Fig. 1). It reaches its largest extension about 50 ms after initiation of the jump, whereupon it shrinks and decays. In the example shown (Fig. 1B), the area in the meridional plane within which the vorticity exceeds 1 s^{-1} peaks at about 3 mm^2, corresponding to an equivalent circular radius of the vortex of about 1 mm and, hence, a diameter of the doughnut-shaped vortex ring of ca. 4 mm. The circulation of the vortex ring reaches its peak value simultaneous with the maximum spatial extension of the eddy, whereupon it declines hyperbolically (Fig. 1A).

The point momentum source model (eq. 3) provides a good fit to the decay phase of the observed circulation (Fig. 1A) and, thus allows us to use the model to estimate the hydrodynamic impulse (I) of the vortex ring (Table 1). Because the momentum of the copepod has to equal the momentum of

the backward jet of water, the magnitude of estimated hydrodynamic impulse of the vortex impulse should be of similar magnitude as the density-specific momentum (M/ρ) of the copepod. The observations are consistent with this, although the vortex impulse in several cases appears to be underestimated (Fig. 2D)

After the wake vortex ring has formed, it grows radially due to diffusion and at the same time translates downstream. As a result of these two processes, the position of the vorticity maximum moves and the movement is generally well described by the point momentum source model (eq. 6; Fig. 1C). For a vortex generated by an instantaneous point force, the center of the vortex and the position of the vorticity maximum separate over time (Appendix A). This separation is rather obvious from visual inspections of vorticity and flow fields (Fig. 2A) and can also be verified quantitatively (not shown), even though it is difficult to accurately define the centre of the vortex.

The body bound vortex

The stopping vortex ring developing around the decelerating copepod rotates opposite the wake vortex, but is of similar magnitude (Fig. 2B). In the two cases (jumps 20-2 and 58) where we analyzed all 2x2 meridional plane sections of the vortex rings, the time evolution of the body bound ring was very similar to that of the wake ring, and the estimated peak circulation of the two vortices were within 5 % of one another.

Extension of the velocity field

The cross-sectional area enveloping fluid velocities exceeding preset threshold magnitudes ($U > U^*$) increases rapidly to a maximum simultaneously with the copepod reaching its peak velocity, and then declines (Fig. 3). Depending on the threshold magnitude the decline is slower than the deceleration of the copepod. High velocities last only very short, whereas velocities > 1 mm s^{-1} are evident ca. 300 ms after jump initiation for the example shown. The duration of a velocity signal

varies approximately in proportion to its maximum areal extension. Signal durations predicted using the point momentum source model (eq. 5) correspond well with the observed durations (Fig. 3B). The peak area with velocities exceeding 1 mm s^{-1} is ca. 10 mm^2, about 50 times the cross-sectional area of the copepod itself for the example shown.

The extension of the area with $U > U^*$ depends on the size and velocity of the copepod, with the latter expressed as the density-specific momentum of the copepod (Fig. 4). For the lower threshold velocities, this area scales with the momentum to a power of near 2/3; for the higher threshold velocities, where velocity contour lines come closer to the copepod, the relations become noisier (Fig. 4A). If the momentum of the copepod is normalized by the threshold velocity, the observations for threshold velocities between 1-3 mm s^{-1} collapse into one relationship (Fig. 4B), with the area of influence proportional to $(M/\rho U^*)^{2/3}$ (Fig. 4B).

DISCUSSION

Vortices are created almost universally when animals move through fluids at Reynolds numbers exceeding 10^2 and vortex formation and dynamics are widely studied for flying and swimming organisms in this Reynolds number regime (see review by Dabiri 2009). In contrast, the vortex ring formed in the wake of copepods performing weak repositioning jumps occurs at lower Reynolds numbers (Table 1). The spatial and temporal dynamics of vortices in viscous dominated fluid differ from those formed at higher Reynolds numbers and are much less studied.

The wake vortex results from viscous diffusion of vorticity in the shear layer of the jet produced by the backward kicking legs. This is a different formation mechanism from the vortices generated due to vortex sheet roll-up in a piston-cylinder apparatus, the classical model system for studies of vortex ring formation (Gharib et al. 1998). Consequently, while inviscid theory has proven useful in the analysis of animal propulsion at higher Re (Dickinson 1996), it does not work in this much

lower Re–range. For example, there is no formation process and it becomes irrelevant to define a formation number, often used to characterize vortex ring formation in both piston/cylinder arrangements and in flying and swimming organisms at high Re (Dabiri 2009).

As an alternative, we proposed here a simple model, an impulsive point force, to characterize the viscous toroidal vortex formed in the wake of the jumping copepod. Overall, our observations are consistent with the predictions of this simple and highly idealized model with respect to spatial extension and temporal decay and translation of the wake vortex, which are all different than would be predicted using inviscid theory. For example, the temporal separation of the position of the vorticity maximum and the vortex center (Fig. 2) is a characteristic specific to these viscous vortices. This observation confirms that the model is relevant to lower Re copepod jumps. Also, the axial travel speed and distance of the wake vortex is much less than inviscid theory would predict. In fact, according to inviscid theory vortex rings with similar spatial dimensions and impulse would travel axially at speeds calculated in 10's of mm s^{-1} (Saffman 1992), while in a typical copepod relocating jump the wake vortex would last < 1-2 s and the total axial travel distance would measure < 1 mm. Finally, we found the circulation of the wake vortex to decay after formation due to viscosity, while inviscid rings may grow and slow down due to entrainment, i.e., by an entirely different dynamics.

Given the inherent difficulty of filming a non-tethered copepods and the low likelihood of jumps being directed exactly perpendicular to the view direction and within the laser sheet and the consequent imperfection of this assumption for any particular jump, we find the quantitative correspondence between model and observations satisfying. It is also re-assuring that the estimates of the magnitudes and decays of the circulation of the two vortex rings are similar but of opposite orientation and, hence, that the net circulation is zero throughout (Kelvin's Law). Thus, the simple model provides a good description of our case, allowing us to use it to extrapolate our observations

and to evaluate much more generally the fluid dynamic signal and the predation risk that ambush feeding copepods experience.

Spatial extension and temporal duration of the fluid velocity signal

The scaling of the extension of the velocity field observed agrees well with that proposed by the simple vortex model (eq. 4), at least in the far field (i.e., for small U^*) (Fig. 4). Strictly speaking, the model applies only to the wake vortex, but as the following loose argument suggests, the predicted scaling may be extended to the entire imposed flow field. The momentum of the forward jumping copepod must be countered by an oppositely directed momentum of the water in the wake. The decelerating copepod, in turn, must 'pay' momentum back to the ambient water, and this would again be of the same magnitude. Because the momentum of the water scales with volume x velocity, it follows that the cross-sectional area - over the entire imposed flow field - with velocity magnitudes exceeding U^* must scale with the momentum of the copepod to a power of 2/3 and with the threshold velocity to power -2/3, as observed (Fig. 4B).

The fluid disturbance generated by the jumping copepod does not last long and by about a ¼ of a second after the jump the fluid disturbance generated by the jump has vanished. The time scale is much shorter than the duration of the fluid disturbance generated by a copepod that performs a powerful escape jump. Duren & Videler (2003) observed a significant fluid signal for more than 2 s after a powerful escape jump of a mm-sized copepod. This size dependency of the signal duration is to be expected, and is governed by the viscous time-scale, L^2/ν, where L is the linear extension of the fluid disturbance. Bigger eddies last longer. The duration of the fluid signal can be explicitly predicted for the wake vortex (eq. 5), and because the durations of the two vortex rings are similar, we can in fact use eq. 5 to estimate the duration of the entire flow field. These estimates accord well with that observed, particularly for the lower threshold velocities (Fig. 3B).

Predation risk and optimal foraging behavior

Feeding exposes a zooplankton to predation risk (Tiselius et al 1997), and the magnitude of the risk depends on the feeding behavior. We can now use the model and our description of the imposed flow field to estimate the distance at which a mechanoreceptory predator may detect an ambush feeding copepod and compare that to estimates for the two other feeding modes, cruising and feeding-current feeding. The strength of the fluid signal to a mechanosensory predator is simply the imposed fluid velocity magnitude (Kiørboe & Visser 1999). The empirical relation (Fig. 4B) describes the areal extension of the velocity field (A) as a function of the momentum of the copepod and the critical flow velocity magnitude:

$$A = 1.82(M/\rho U^*)^{2/3}. \quad (7)$$

Because all pelagic copepods are of similar shape and perform jumps in a manner similar to that described here, we can take this theoretically founded relation to apply more generally.

We may approximate the maximum detection distance to an ambush feeder (R_A) by the equivalent circular radius of this area. Replacing in eq. 7 the copepod momentum with the product of its mass ($4/3\pi\, a^2\rho$) and jump velocity, v_j, we get

$$R_A = 1.23a\left(\frac{v_j}{U^*}\right)^{1/3} \quad (8)$$

where a is the equivalent radius of the copepod (approximately ¼ of its length) and U^* can be interpreted as the threshold signal strength required for detection. As a first order approximation, similar expressions for hovering and cruising grazers, modeled as a stokeslet and a dipole, respectively, are (Kiørboe 2010)

$$R_C = a\left(\frac{v}{U^*}\right)^{1/2} \tag{9}$$

$$R_H = a\left(\frac{v}{U^*}\right) \tag{10}$$

The reaction distance to the jumping copepod refers only to the peak signal immediately following the jump. For comparison with the more continuous signals of the two other feeding modes, it may be more relevant to consider the time-averaged detection distance. To estimate that we need to know the duration of the signal, t^* (eq. 5), and the jump frequency (f); the time-averaged signal then scales with $t^* f R_A$.

We may estimate the jump frequency of an ambush feeding copepod by assuming that jumping should exactly counter sinking; hence f = sinking velocity/jump distance. One-beat repositioning jumps invariably brings the copepod ca. 2 body lengths forward, independent of the size of the copepod and the duration of the power stroke (Kiørboe et al. 2010). Sinking velocity should increase with copepod length squared (Stokes law) and, hence, jump frequency with length. Observed sinking velocities indeed show approximately this scaling, and predicted jump frequencies of ambush feeding copepods and copepod nauplii conform largely with the expectation, while cruisers and feeding-current feeders jump much less frequently (Fig. 5). Combining the scaling properties of reaction distance (eq. 8), jump frequency, and signal duration (eq. 5), the time averaged detection distance increase with $a^3(v_j/U^*)$, that is, dramatically with the size of the

copepod and much faster than is the case for cruising and hovering copepods. (Fig. 6A). Using a simple ballistic predator-prey encounter model, these considerations further demonstrate that ambush feeding becomes increasingly risky for larger copepods (Fig. 6B).

Optimal foraging behavior is the result of a compromise between gains and risks associate with a particular foraging mode (Lima & Dill 1990; McNamara & Houston 1992). Ambush feeding is inherently less efficient than the more active feeding modes, simply because the encounter velocity is governed by the swimming velocity of the prey for the former and by the (higher) velocity of the grazer for the latter (Kiørboe 2010). While the above considerations of predation risk associated with the different feeding behaviors are correct only in an order of magnitude sense, they do suggest that the lower predation risk experienced by small ambush feeding copepods makes this relatively inefficient feeding strategy feasible. Lower predation risks of ambush feeders has been assumed in models of optimal foraging in zooplankton (e.g. Visser 2007), and do conform with field observations suggesting that mortality rates of ambush feeding copepods are much lower than mortalities of similarly sized copepods with more active feeding strategies (Eiana & Ohman 2004). However, the relative advantage of ambush feeders in terms of low predation risk applies only to small copepods. Depending on the predator landscape, ambush feeding in larger copepods becomes similarly or more risky than other feeding modes (Fig. 8). The primary group of obligate ambush feeding copepods in the ocean belong to the genus *Oithona* (Paffenhöfer 1995), and these are all small, typically < 1 mm. Intermediate sized copepods, such as *Acartia tonsa*, may switch between

ambush and feeding-current feeding (Jonsson & Tiselius 1990) while copepods larger than 1-1.5 mm all appear to be cruise- or feeding-current feeders (e.g.; *Calanus* spp.).

In conclusion, our quantitative description of the fluid dynamics of repositioning jumps by copepods have enabled us to predict the hydrodynamic signature of ambush feeding and has demonstrated the significance of hydrodynamics in understanding the ecology and behavior of small plankton operating at low Re. Previous work has focused on inviscid vortices in the context of animal propulsion, which is irrelevant in the viscous world of the plankton. Many ecologically important marine organisms, including most zooplankton, small fish larvae, and even krill operate in the low Reynolds number regime (Re 0.1-200) and their propulsion and hydrodynamic signaling may similarly be governed by the viscous vortices that may form as a result of their motion.

Acknowledgements. We enjoyed conversations with Tim Pedley. TK was supported by a grant from the Danish Research Council and by a Niels Bohr Fellowship to TK and HJ was supported by National Science Foundation grants NSF OCE-0352284 & IOS-0718506.

REFERENCES

Afanasyev, Y. D. 2004 Wakes behind towed and self-propelled bodies: asymptotic theory. Phys. Fluids 16, 3235-3238.

Buskey, E. J., Lenz, P. H. & Hartline, D. K. 2002 Escape behaviour of planktonic copepods in response to hydrodynamic disturbances: high speed video analysis. *Mar. Ecol. Prog. Ser.*, **235**, 135-146.

Berg, H. C. 1993 *Random Walks in Biology*, 2nd ed. Princeton University Press, Princeton

Catton, K. B., Webster, D. R., Brown, J., & Yen, J. 2007 Quantitative analysis of tethered and free-swimming copepodid flow fields. *J. Exp. Biol.*, **210,** 299-310.

Dabiri, J. O. 2009 Optimal vortex formation as a unifying principle in biological propulsion. *Ann. Rev. Fluid. Mech.,* **41**, 17-33.

Dickinson, M. H. 1996 Unsteady mechanisms of force generation in aquatic and aerial locomotion. *Amer. Zool.,* **36,** 537-554.

Duren, L. A. van & Videler, J. J. 2003 Escape from viscosity: the kinematics and hydrodynamics of copepod foraging and escape swimming. *J. Exp. Biol*., **206**, 269-279.

Eiane, K. &. Ohman, M. D. 2004 Stage-specific mortality of *Calanus finmarchicus*, *Pseudocalanus elongatus* and *Oithona similis* on Fladen Ground, North Sea, during a spring bloom, *Marine Ecology-Progress Series*, **268,** 183-193.

Feigenbaum, D. & Reeve, M. R. 1977 Prey Detection in the Chaetognatha: Response to a Vibrating Probe and Experimental Determination of Attack Distance in Large Aquaria. *Limnol. Oceanogr.* **22,** 1052-1058.

Fields, D. M. & Yen, J. 1997 The escape behavior of marine copepods in response to a quantifiable fluid mechanical disturbance. *J. Plankton Res.* **19**, 1289-1304.

Fenchel, T. & Hansen, P. J. 2006 *Motile behaviour of the bloom-forming ciliate Mesodinium rubrum*. *Mar. Biol. Res.* **2,** 33-40.

Gharib, M., Rambod, E., & Shariff, K. 1998 A universal time scale for vortex ring formation. *J. Fluid Mech.* **360,** 121-140.

Jakobsen, H. H., Everett, L. M., & Strom, S. L. 2006 Hydromechanical signaling between the ciliate Mesodinium pulex and motile protist prey. *Aquat. Microb. Biol.* **44,** 197-206.

Jonsson, P. R., & Tiselius, P. 1990 Feeding behavior, prey detection and capture efficiency of the copepod *Acartia tonsa* feeding on planktonic ciliates. *Mar. Ecol. Prog. Ser.* **60,** 35-44.

Jiang, H. S., Meneveau, C., & Osborn, T. R. 2002 The flow field around a freely swimming copepod in steady motion. Part II: Numerical simulation. *J. Plankton Res.* **24,** 191-213.

Jiang, H. S., & Paffenhöfer, G. A. 2008 Hydrodynamic signal perception by the copepod *Oithona plumifera*. *Mar. Ecol. Prog. Ser.* **373,** 37-52

Kiørboe, T. 2010 How zooplankton feed: Mechanisms, traits and tradeoffs. *Biol. Rev.* in press

Kiørboe, T., Andersen, A., Langlois, V. J., & Jakobsen, H. J. (2010). Unsteady motion: Escape jumps in copepods, their kinematics and energetics. J. R. Soc. Interface in press

Kiørboe, T., Andersen, A., Langlois, V., Jakobsen, H. H., & Bohr, T. 2009 Mechanisms and feasibility of prey capture in ambush feeding zooplankton. *Proc. Natl. Acad. Sci.* **106,** 12394-12399.

Kiørboe, T., & Visser, A. W. 1999 Predator and prey perception in copepods due to hydromechanical signals. *Mar. Ecol. Prog. Ser.* **179,** 81-95.

Langlois, V., Andersen, A., Bohr, T., Visser, A. & Kiørboe, T. 2009 Significance of swimming and feeding currents for nutrient uptake in osmotrophic and interception feeding flagellates. *Aquat. Microbiol*. **54,** 35-44.

Lenz, P. H., Hower, A. E. & Hartline, D. K. 2004 Force production during pereiopod power strokes in *Calanus finmarchicus*. *J. Mar. Systems* **49,** 133-144.

Leptos. K. C., Guasto, J. S., Gollub, J. P., Pesci, A. I. & Goldstein, R. E. 2009. Dynamics of Enhanced Tracer Diffusion in Suspensions of Swimming Eukaryotic Microorganisms. *Phys Rev. Lett.* **103,** 198103.

Malkiel, E., Sheng, I., Katz, J. & Strickler, J. R. 2003 The three-dimensional flow field generated by a feeding calanoid copepod measured using digital holography. *J. Exp. Biol.* **206,** 3657-3666.

Lima, S. L., & Dill, L. M. 1990 Bahavioral decisions made under the risk of predation: A review and prospectus. *Can. J. Zool.* **68,** 619-640.

McNamara, J. M., & Houston, A. I. 1992 Risk-sensitive foraging: A review of the theory. *Bull. Math. Biol.* **54,** 255-378.

Paffenhöfer, G. A. & Mazzocchi, M. G. 2002 On some aspects of the behaviour of *Oithona plumifera* (Copepoda : Cyclopoida). *J. Plankton Res.* **24,** 129-135.

Saffman, P. G. 1992 *Vortex Dynamics*. Cambridge University Press.

Svensen, C., & Kiørboe, T. 2000 Remote prey detection in *Oithona similis*: hydromechanical vs. chemical cues. *J. Plankton Res.* **22,** 1155-1166.

Tiselius, P. & Jonsson, P. R. 1990 Foraging behaviour of six calanoid copepods: observations and hydrodynamic analysis. *Mar. Ecol. Prog. Ser.* **66,** 23–33.

Tiselius,P., Jonsson, P. R., Kaartvedt, S., Olsen, M. E & Jarstad, T. 1997 Effects of copepod foraging behavior on predation risk: An experimental study of the predatory copepod *Pareuchaeta norvegica* feeding on *Acartia clausi* and *A. tonsa* (Copepoda). *Limnol. Oceanogr.* **42,** 164-170.

Titelman, J. & Kiørboe, T. 2003 Motility of copepod nauplii and implications for food encounter. *Mar. Ecol. Prog. Ser.* **247,** 123-135.

Visser, A. W. 2001 Hydromechanical signals in the plankton. *Mar. Ecol. Prog. Ser.* **222,** 1-24.Visser, A. W. 2007 Motility of zooplankton: fitness, foraging and predation. *J. Plankton Res.* **29,** 447-461.

Yen, J. & Strickler, J. R. 1996 Advertisment and concealment in the plankton: what makes a copepod hydrodynamically conspicuous? *Inv. Biol.* **115,** 191-205.

LEGENDS FOR FIGURES

Fig. 1. Example of formation, decay, extent, and translation of the wake vortex. A: Temporal variation in the velocity of the copepod, the duration of the active stroke phase, and the observed circulation of the eddy together with a least square fit of equation 3 to the decaying phase of the vortex circulation. B: Area of a wake eddy with vorticities exceeding threshold magnitudes. C: Translation of the vorticity maximum position with a fit of equation 6. (A,B: jump 20-2; C: jump 78, Table 1).

Fig. 2. Instantaneous flow and vorticity fields (A & C) around jumping copepod 29 ms after initiation of the jump, and the vorticity field averaged over 250 ms (B). The black arrows in (A) show the approximate position around which the water circulates (vortex center). (Jump 20-2, Table 1). D: Hydrodynamic impulse of the wake vortex estimated from the temporal decay of the circulation (Eq. 3, Fig. 1A) as a function of the density-specific momentum of the copepod.

Fig. 3. A: Duration of the power stroke, temporal variation in velocity of the copepod, and the net distance moved as a function of time. B: Temporal variation in the extension of the cross-sectional area within which the induced flow velocity exceeds certain threshold magnitudes, U^*. Triangles show the duration of fluid velocities exceeding the threshold as predicted from the momentum of the copepod (eq. 5) (Jump 58, Table 1); same color code as the graphs.

Fig. 4. Peak areas with induced flow velocities exceeding thresholds velocities (U^*) as a function of the density-specific momentum of the copepod (A), or the specific momentum normalized by the threshold velocity (B). Individual regression lines have been plotted in (A), and a regression

including only threshold velocities of 1-3 mm s^{-1} and forced with a slope of 2/3 have been computed in (B). This regression is Log (Area, mm^2) = Log (1.815) + (2/3) x Log ($M/\rho U^*$, mm^3); $R^2 = 0.83$. Only jumps where the entire imposed flow field was within the field of view are included (n=12).

Fig. 5. Sinking velocities (A) and jump frequencies (B) of copepods and copepod nauplii reported in the literature. In (B) the predicted jump frequency is sinking velocity divided by 2 body lengths per jump. The lines in (A) are regression lines relating sinking velocity (v_{sink}, mm s^{-1}) to body length (L, mm); for nauplii: Log (v_{sink}) = 0.21+1.4 Log(L); for copepods: Log (v_{sink}) = -0.12+1.9 Log(L) Data are from Tiselius & Jonsson (1990), Jonsson & Tiselius (1990), Svensen & Kiørboe (2000), Paffenhöfer & Mazzocchi (2002), and Titelman & Kiørboe (2003).

Fig. 6. Predator detection distances (A) and relative mortalities (B) of copepods with different feeding strategies towards cruise (full lines) or ambush predators (dotted lines) that perceive their copepod prey from the hydrodynamic disturbance that it generates. Detection distances computed from eqs. 8-10; for ambush feeding copepods the time-averaged detection distance is 0.5·jump frequency·t^*·R_A. Jump frequency ($f = v_{sink}/2L$; L = prosome length) was computed assuming a size-dependent sinking velocity (Fig. 6). Jump velocity, v_j, was assumed to scale with $L^{0.67}$ (Lenz et al. 2004) and equal 100 mm s^{-1} for a 1-mm sized copepod. Cruise and feeding current velocities, v, were assumed identical and estimated from the data compilation in Kiørboe et al. (2010), Log (v, mm s^{-1}) = 0.38 + 0.93 Log (L, mm). The distinct bend on the curve for ambush feeding copepods occurs when the signal duration exceeds the time between jumps (i.e., $t^*f > 1$). Relative predation mortality was computed as $\pi R^2(v^2+u^2)^{0.5}$, where u is the predator velocity, taken to be $10v$ for a cruise predator. Copepod prey velocities (v) were assumed zero for ambush feeding and hovering

copepods. Relative predation mortality of ambush feeding copepods to ambush feeding predators were computed assuming diffusive encounters, as $4\pi DR$, where $D = 2/3\ L^2 f$ (Berg 1993). A critical signal strength for the prey detection was assumed, $U^* = 0.1$ mm s^{-1}.

Table 1. Summary statistics for 16 analysed copepod jumps. Copepod size is prosome length; U_{max} is the maximum speed of copepod; Re is the Reynolds number of the copepod (= U_{max} x 0.38 x length/viscosity), where 0.38 is the aspect ratio of the copepod prosome; τ is the duration of the power stroke(s); Copepod momentum was U_{max} x copepod volume, where the volume was computed by assuming the shape of a prolate sphere with length equal to prosome length and short axes equal 0.38 x length.

Jump #	Copepod length mm	U_{max} mm s^{-1}	Re	τ ms	Peak vortex circulation mm^2s^{-1}	Momentum of copepod mg mm s^{-1}	Vortex impulse mm^4s^{-1}	Number beat cycles	comment
12	0.97	173	64	7	17	10.3	7.7	1	
17	1.08	170	70	9	22.3	14.0	19.2	1	
20-1	1.04	208	82	10	14	15.3	8.8	1	
20-2	1.04	200	79	7	15	14.7	8.2	1	
26	0.93	89	31	16	5.4	4.6	4.2	1	
29	1.13	131	56	15	5.7	12.4	5.0	1	
34	0.99	82	31	12	6.5	5.2	3.6	1	
39-1	0.85	326	105	6	13	13.1	4.6	2	Jump out of view
49	0.7	80	21	16	3.2	1.8	3.6	1	
58	1.11	130	55	16	13	11.6	11.9	1	
69	0.72	160	44	15	5.7	3.9	4.0	2	
73-2	1.12	172	73	23	31	15.8	18.6	3	
78	1.04	383	151	15	51.5	28.2	24.6	2	Jump out of view
83	1.03	168	66	11	36.2	12.0	10.4	1	
88	0.97	273	101	22	15.6	16.3	6.2	3	Jump out of view
93	0.97	188	69	8	23	11.2	9.22	1+	Jump out of view

Fig. 1

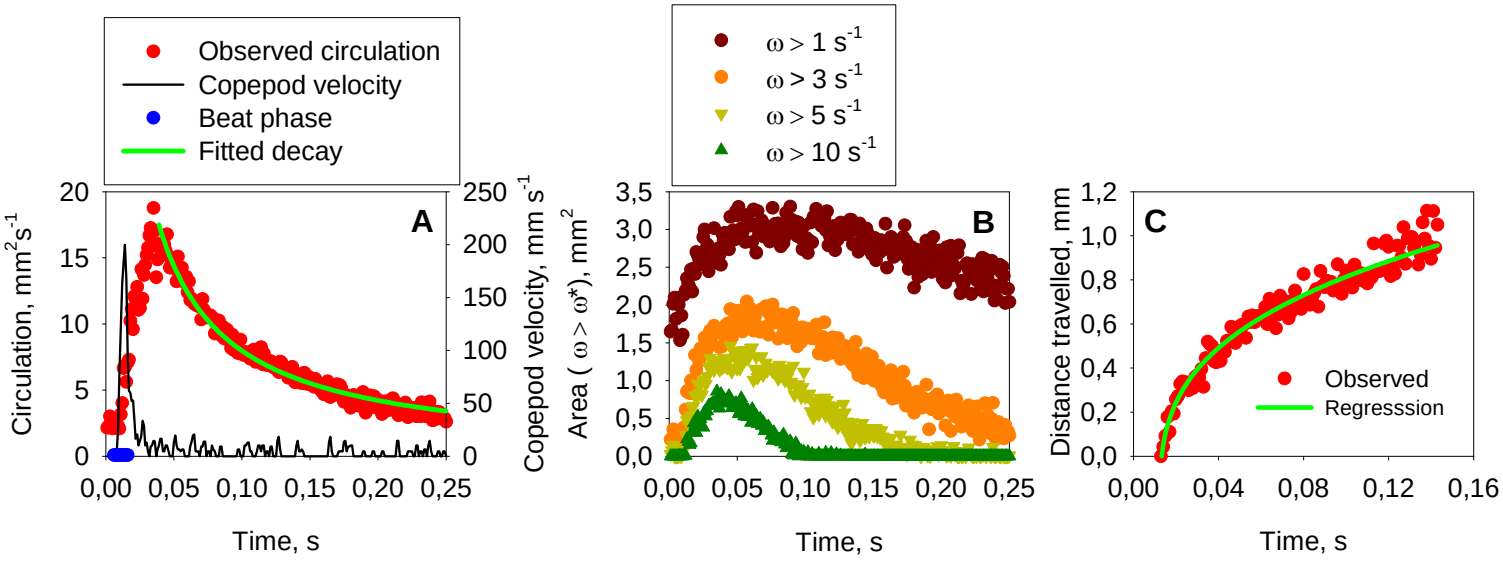
Observed circulation
Copepod velocity
Beat phase
Fitted decay
A
Circulation, mm²s⁻¹
Copepod velocity, mm s⁻¹
Time, s
ω > 1 s⁻¹
ω > 3 s⁻¹
ω > 5 s⁻¹
ω > 10 s⁻¹
B
Area (ω > ω*), mm²
Time, s
C
Distance travelled, mm
Observed
Regresssion
Time, s

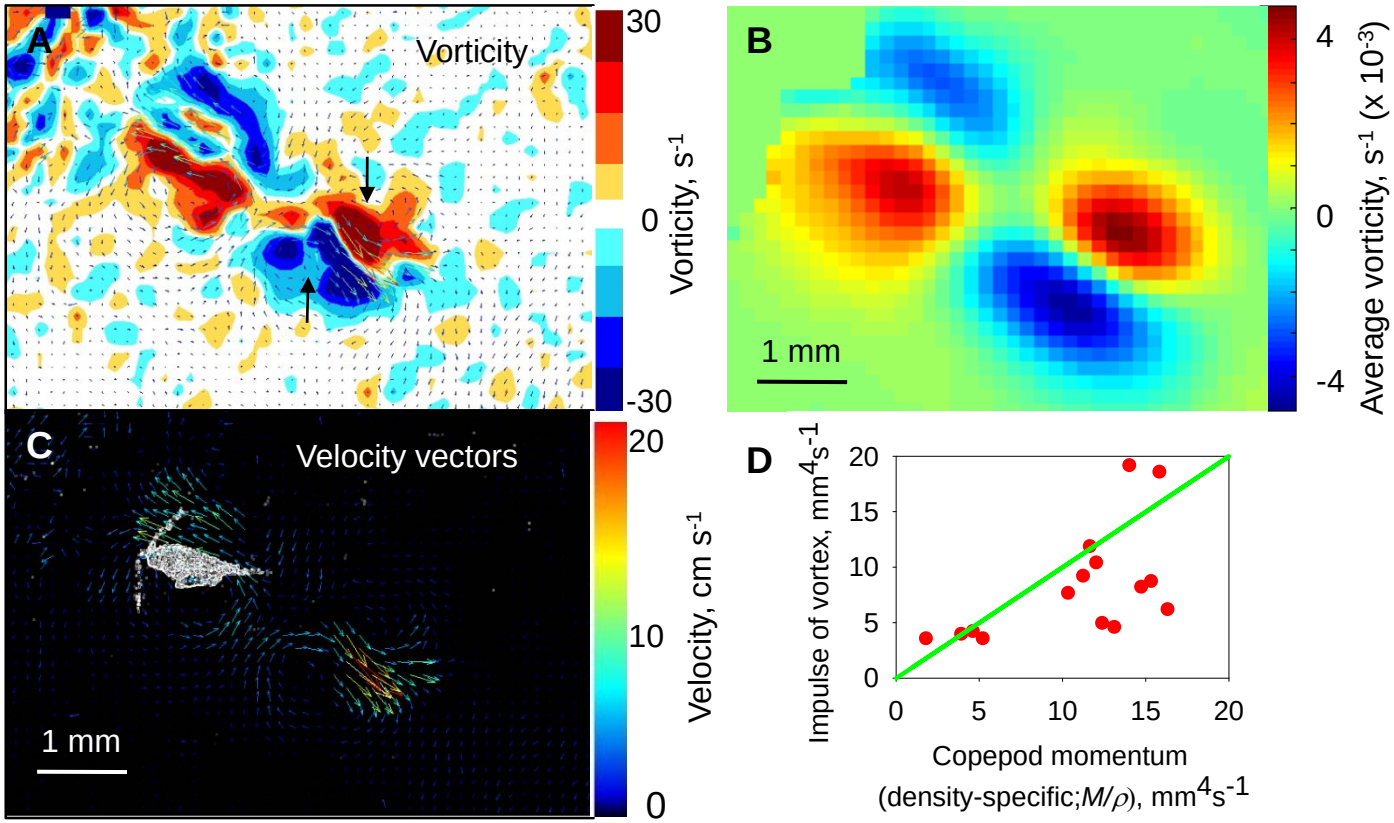
A
Vorticity
30
0
-30
Vorticity, s-1
B
1 mm
4
0
-4
Average vorticity, s-1 (x 10-3)
C
Velocity vectors
1 mm
20
10
0
Velocity, cm s-1
D
Impulse of vortex, mm4s-1
0
5
10
15
20
Copepod momentum
(density-specific;M/ρ), mm4s-1

Fig. 2

Figure 3

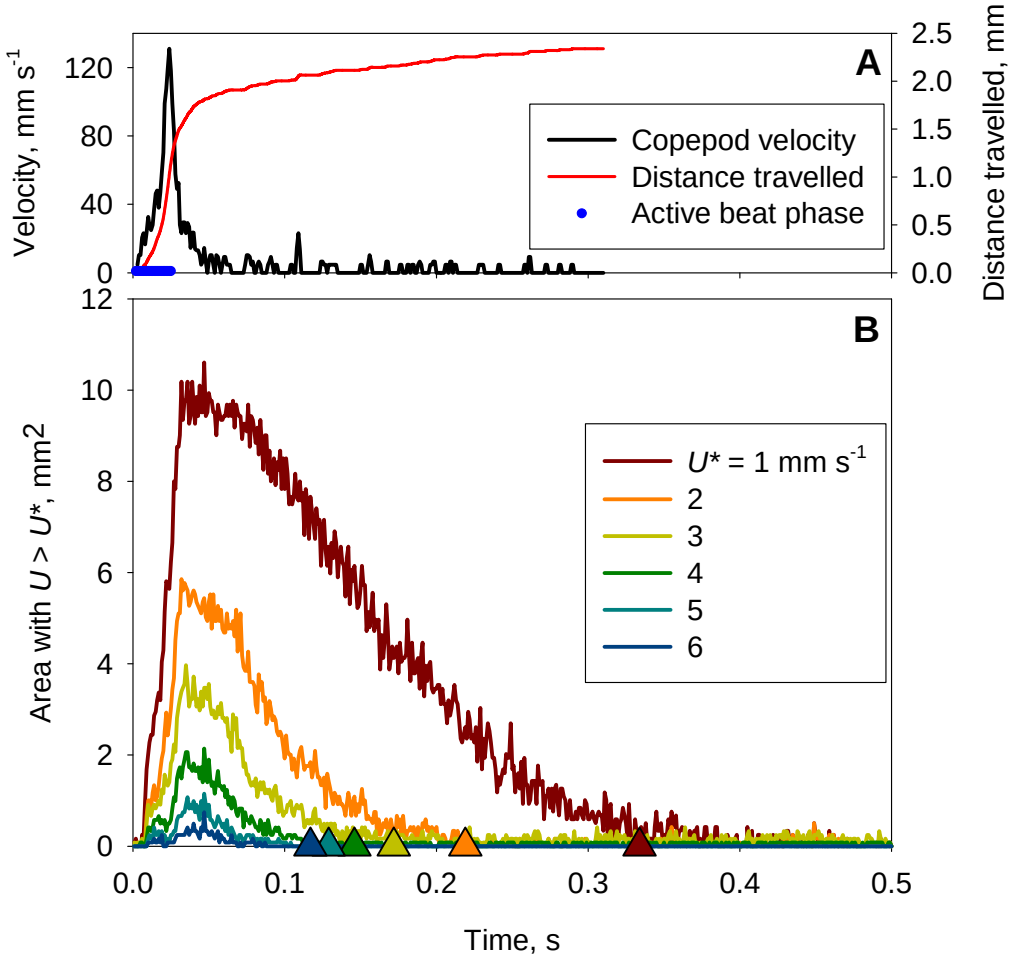
A
Velocity, mm s-1
120
80
40
0
2.5
2.0
1.5
1.0
0.5
0.0
Distance travelled, mm
Copepod velocity
Distance travelled
Active beat phase
B
Area with U > U*, mm2
12
10
8
6
4
2
0
U* = 1 mm s-1
2
3
4
5
6
0.0
0.1
0.2
0.3
0.4
0.5
Time, s

Figure 4

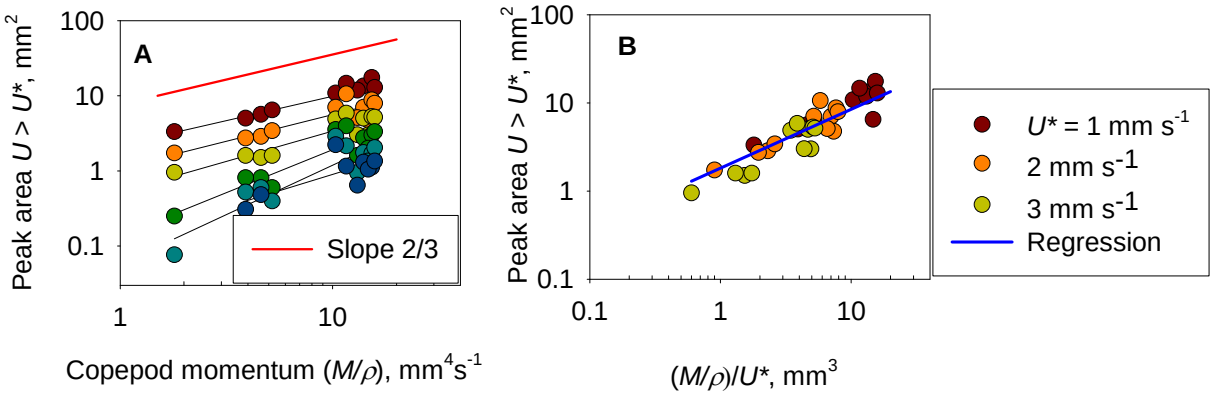
A
B
100
10
1
0.1
0.1
1
10
Peak area U > U*, mm2
Slope 2/3
Copepod momentum (M/ρ), mm4s-1
(M/ρ)/U*, mm3
U* = 1 mm s-1
2 mm s-1
3 mm s-1
Regression

Figure 5

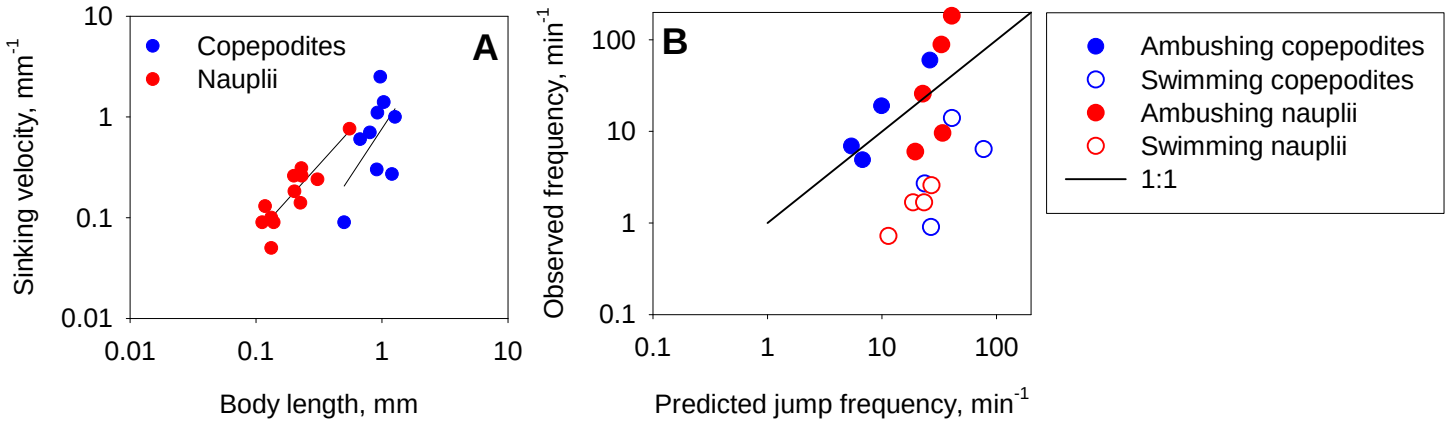
Sinking velocity, mm-1
10
1
0.1
0.01
0.01
0.1
1
10
Body length, mm
Copepodites
Nauplii
A
Observed frequency, min-1
100
10
1
0.1
0.1
1
10
100
Predicted jump frequency, min-1
B
Ambushing copepodites
Swimming copepodites
Ambushing nauplii
Swimming nauplii
1:1

Figure 6

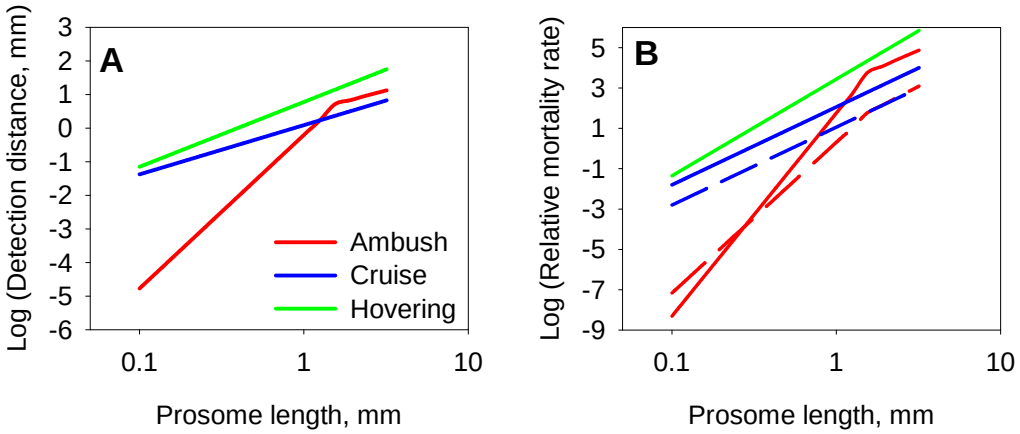
A
B
Log (Detection distance, mm)
Log (Relative mortality rate)
Prosome length, mm
Prosome length, mm
Ambush
Cruise
Hovering
3
2
1
0
-1
-2
-3
-4
-5
-6
5
3
1
-1
-3
-5
-7
-9
0.1
1
10
0.1
1
10

ELECTRONIC SUPPLEMENTARY MATERIAL

For Kiørboe, T., Jiang, H., & Colin, S. P. *Danger of zooplankton feeding: The fluid signal generated by ambush feeding copepods*

Appendix A. **Vortex ring generated by impulsive point force**

We use the solution of a viscous vortex ring generated by an impulsive point force to describe the toroidal vortex left in the wake of the jumping copepod.

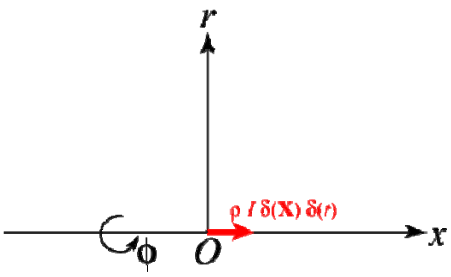

Fig. A1. A meridional plane belonging to a cylindrical polar coordinate system (x, r, ϕ), where ϕ is the azimuthal coordinate. A point momentum source acts impulsively for a very short period of time [formally represented by the Dirac delta function $\delta(t)$] in the positive x-direction (red arrow).

Formation and decay of the vortex: Consider a point momentum source applied at the origin O of the cylindrical polar coordinate system (Fig. A1). The point momentum source acts impulsively and imparts locally a finite momentum ρI to the fluid (where ρ is the mass density of the fluid and I the hydrodynamic impulse.). For the 3-dimensional axisymmetric flow, the dimensions of the hydrodynamic impulse are L^4T^{-1}.

Vorticity ( ) and streamfunction ( ) for the flow have been obtained using Stokes approximation (e.g., Afanasyev 2004):

(A1)

(A2)

where $\xi = \sqrt{\frac{x^2+r^2}{4\nu t}}$ and ν the kinematic viscosity. The components of velocity in the meridional plane are given from the streamfunction by

$$u = \frac{1}{r}\frac{\partial \psi_\phi}{\partial r} \tag{A3}$$

$$v = -\frac{1}{r}\frac{\partial \psi_\phi}{\partial x} \tag{A4}$$

where *u* and *v* are the velocity components in the axial (*x*-) and the radial (*r*-) directions, respectively.

Integrating the vorticity (ω_ϕ) distribution over the whole meridional plane leads to a quite simple formula for the circulation and decay of the vortex ring:

$$\Gamma(t) = \int_{-\infty}^{+\infty}\int_{0}^{+\infty} \omega_\phi \, dx \, dr = \frac{I}{4\pi\nu t} \tag{A5}$$

One can also show that:

$$I = \pi \int_{-\infty}^{+\infty}\int_{0}^{+\infty} \omega_\phi \, r^2 dx \, dr \tag{A6}$$

which is the definition of the hydrodynamic impulse for axisymmetric flows. *I* is conserved even in the presence of viscosity but in the absence of body forces (Saffman 1992).

Spatial extension of the flow field: At small time the far field (i.e. $\xi >> 1$) of the flow is approximately irrotational (potential) and behaves as:

$$\psi_\phi = \frac{I}{4\pi}\frac{r^2}{(x^2+r^2)^{3/2}} \tag{A7}$$

Substituting (A7) into (A3)-(A4), one obtains the two velocity components:

$$u = \frac{I}{4\pi}\frac{2x^2-r^2}{(x^2+r^2)^{5/2}} \tag{A8}$$

$$v = \frac{I}{4\pi}\frac{3xr}{(x^2+r^2)^{5/2}} \tag{A9}$$

The associated velocity magnitude is:

$$U = \sqrt{u^2+v^2} = \frac{I}{4\pi}\frac{\sqrt{4x^2+r^2}}{(x^2+r^2)^2} \tag{A10}$$

From (A10), one can determine the size (R^*) of the domain, with flow velocity greater than a threshold velocity U^*, occupied by the vortical flow structure left behind the jumping copepod right after the jump is initiated. Directly behind the jumping copepod the extension in the *x*-direction (*r* = 0) is

$$R_x^* = \left(\frac{1}{2\pi} \frac{I}{U^*} \right)^{1/3} \tag{A11}$$

and in the lateral *r*-direction (*x* = 0)

$$R_r^* = \left(\frac{1}{4\pi} \frac{I}{U^*} \right)^{1/3} \tag{A12}$$

Similarly, for large time (i.e. $\xi \to 0$), one can show that the flow velocity magnitude is approximately:

$$U = \frac{2I}{3\pi^{3/2}} \frac{1}{(4\nu t)^{3/2}} \tag{A13}$$

Translation of the vortex: A characteristic feature of a viscous vortex ring generated by a momentary point force is that the vorticity maximum and the center of the vortex (flow rotation center) separate in the radial direction over time. It follows from the Stokes solution that the vorticity maximum travels along the *r*-axis with its *r*-position evolving as:

$$r_\omega(t) = \sqrt{2\,\nu t} \tag{A14}$$

and the vortex center simultaneously moves in the *r*-direction as:

$$r_u(t) = 3.0224370\,\sqrt{\nu t} \tag{A15}$$

Therefore, the separation distance evolves as

$$\Delta r(t) \equiv r_u(t) - r_\omega(t) = 1.6082234\,\sqrt{\nu t} \tag{A16}$$

The Stokes solutions (A1)-(A2) do not allow for the Stokes vortex ring to drift along the *x*-axis. However, vorticity moves with the fluid and so the vortex ring will advect downstream at a rate that depends on the hydrodynamic impulse, *I*. The small time *x*-displacement of the axisymmetric vortex ring for the impulsive point force may be approximated by (Afanasyev & Korabel 2004):

$$\Delta x(t) = \left(\frac{2I}{\pi}\right)^{1/4} (t - t_0)^{1/4} \qquad \text{(A17)}$$

References

Afanasyev, Y. D. 2004 Wakes behind towed and self-propelled bodies: asymptotic theory. *Phys. Fluids* **16**, 3235-3238.

Afanasyev, Y. D. & Korabel, V. N. 2004 Starting vortex dipoles in a viscous fluid: asymptotic theory, numerical simulations and laboratory experiments. *Phys. Fluids* **16**, 3850-3858.

Saffman, P. G. 1992 *Vortex Dynamics*. Cambridge University Press.

Legend for Appendix movie 1

Reposition jump of *Acartia tonsa* (lower right corner) and the measured vorticity (contours) and velocity (arrows) fields. The movies are shown in Slow motion (35 x real time).